Supplementary Document: Effect of nearby Metals on Electro-Quasistatic Human Body Communication

Samyadip Sarkar, Arunashish Datta, David Yang, Mayukh Nath
Student Member, IEEE, Shovan Maity, *Member, IEEE* and Shreyas Sen, *Senior Member, IEEE*

I. Transfer Function Derivation for Proximity-based Interaction with Ground-connected Metallic Object

The simplified circuit model for the proximity-based interaction between EQS HBC user and a ground-connected metallic object is presented in Supplementary Fig. 1. For the return path capacitances at the Tx and Rx, we define the return path capacitances in the absence of any surrounding conductive objects such as C_{xTx} and C_{xRx}. These values depend on the location of the devices (x) on the subject's body and the geometry of the devices, represented as C_{self}. Specifically, the return path capacitances are expressed in Eqs. 1, 1a.

$$C_{xTx} = xC_{selfTx} \tag{1}$$

$$C_{xRx} = xC_{selfRx} \tag{1a}$$

To distinguish between scenarios where ground-connected metallic objects are present and those where they are absent, we denote the net return path capacitance as C_{retTx} and C_{retRx}. These are mathematically expressed in Eqs. 2, 2a.

$$C_{retTx} = C_{xTx} + C_{GMTx} \tag{2}$$

$$C_{retRx} = C_{xRx} + C_{GMRx} \tag{2a}$$

Here, C_{GMTx} and C_{GMRx} represent the capacitances associated with the ground of the transmitter to the metallic object and from the ground of the receiver to the metallic object, respectively. Assuming C_B as the capacitance between the subject's body and Earth's ground when no other conductive objects are present in the surroundings. It is important to note that the presence of ground-connected metallic objects influences the subject's body capacitance. To differentiate between scenarios in which ground-connected metallic objects are present and those in which they are absent, we denote the net body capacitance (including ground-connected metals) as C_{Body}. This is expressed mathematically in Eq. 3.

$$C_{Body} = C_B + C_{BM} \tag{3}$$

where C_{BM} represents the capacitance between the subject's body and the metallic object. Assuming the effect of inter-device coupling capacitance ($C_C < 1$ fF) to be negligible for Tx and Rx at more than 50 cm apart. The return path impedance being orders of magnitude higher than the impedance contribution of Z_{Body} i.e., $Z_{Body} << Z_{ret}$, the induced potential on subject's body (V_B) is formulated in Eq. 4.

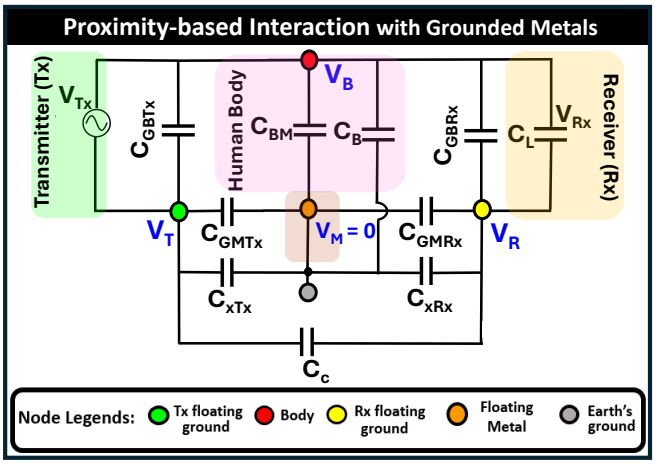

Fig. 1: Simplified equivalent circuit model for proximity-based interaction between subject and ground-connected metals.

$$V_B = \frac{Z_{Body}}{Z_{Body} + Z_{retTx}} V_{Tx} \approx \frac{Z_{Body}}{Z_{retTx}} = \left(\frac{C_{retTx}}{C_B}\right) V_{Tx} \tag{4}$$

Now, a fraction of V_B gets picked-up at the receiver and the received voltage (V_{Rx}) as a function of V_B is presented in Eq. 5.

$$V_{Rx} = \frac{Z_{L(eff.)}}{Z_{L(eff.)} + Z_{retRx}} V_{Tx} \approx \frac{Z_{L(eff.)}}{Z_{retRx}} = \left(\frac{C_{retRx}}{C_{L(eff.)}}\right) V_B \tag{5}$$

"This work was supported by Quasistatics, Inc. under Grant 40003567
Samyadip Sarkar, Arunashish Datta, David Yang, Mayukh Nath, Shreyas Sen are with Elmore Family School of Electrical and Computer Engineering, Purdue University, West Lafayette, IN, USA (e-mail: {sarkar46, datta30, yang996, shreyas}@purdue.edu, nathm@alumni.purdue.edu).
Shovan Maity is with Quasistatics Inc. USA (e-mail: shovan@10xar.com).

Hence, the transfer function is formulated by combining Eq. 4 and Eq. 5 and is presented in Eq. 6.

$$T_{NTGM}(s) = \frac{V_{Rx}}{V_{Tx}}(s) \approx \frac{Z_{Body}}{Z_{retTx}} \times \frac{Z_{L(eff.)}}{Z_{retRx}} \approx \frac{C_{retTx}}{C_{Body}} \times \frac{C_{retRx}}{C_{L(eff.)}} \quad (6)$$

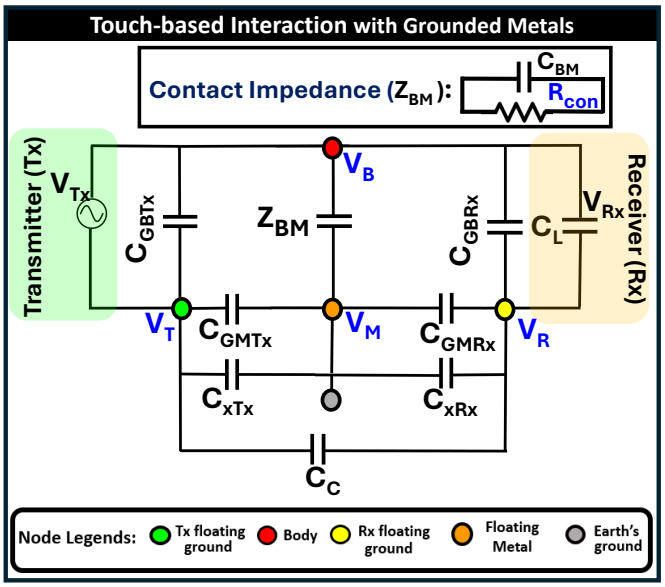

Fig. 2: Simplified equivalent circuit model for touch-based interaction between subject and ground-connected metallic obejcts.

II. Transfer Function Derivation for Touch-based Interaction with Ground-Connected Metallic Object

For the touch-based interaction with ground-connected metallic object, the impedance (Z_{BM}) between the body and the grounded metallic object considered to be the parallel combination of the contact resistance (R_{con}) and the contact capacitance (C_{BM}), shown in the equivalent circuit model in Supplementary Fig. 2. Hence, the expression for Z_{BM} is formulated in Eq. 7.

$$Z_{BM}(s) = \frac{R_{con}}{1 + sR_{con}C_{BM}} \quad (7)$$

Now, in the impedance based transfer function derived in Eq. 6, substituting the value of Z_{BM}, we get the transfer function for touch-based interactions (T_{TGM}), derived in Eq. 8.

$$T_{TGM}(s) = \frac{V_{Rx}}{V_{Tx}}(s) \approx \frac{\frac{R_{con}}{1+sR_{con}C_{BM}}}{\frac{1}{sC_{retTx}}} \times \frac{\frac{1}{sC_{L(eff.)}}}{\frac{1}{sC_{retRx}}} \approx \left(\frac{C_{retTx}C_{retRx}}{C_{L(eff.)}C_{BM} + \left(\frac{C_{L(eff.)}}{sR_{con}}\right)} \right) \quad (8)$$

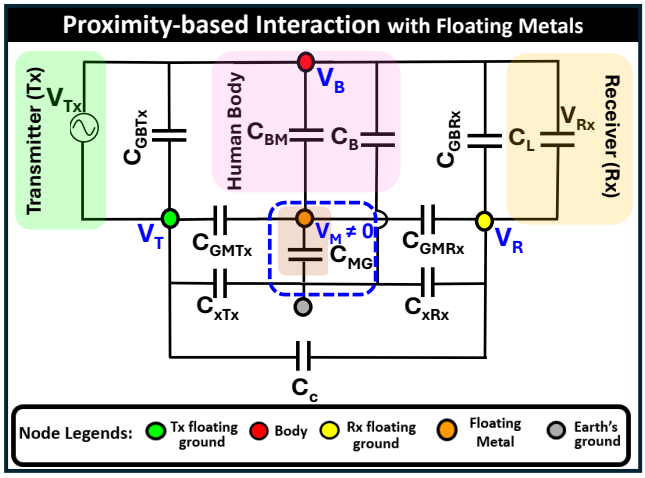

Fig. 3: Simplified equivalent circuit model for touch-based interaction between subject and Floating metallic obejcts.

III. Transfer Function Derivation Proximity & Touch-based Interaction with Floating Ground Metallic Object

The circuit model illustrating the proximity-based interaction between a user of EQS HBC and a floating metallic object is shown in Supplementary Fig. 3. Assuming the voltages at the following nodes: ground of the Tx, ground of the Rx, subject's body, and metal object are at potential V_T, V_R, V_B, and V_M respectively. Applying Kirchhoff's Current Law (KCL) at the node with potential V_T, equation relating these above four nodal voltages is expressed in Eq. 9.

$$(C_B + C_{BM})V_B + (C_{xTx} + C_{GMTx})V_T - C_{L(eff.)}V_R - (C_{GMTx} + C_{BM})V_M = 0 \quad (9)$$

Similarly, by KCL at the earth's ground node, we get the relation expressed in Eq. 10.

$$C_B V_B + C_{xTx}V_T + C_{xRx}V_R + = 0 \quad (10)$$

Then, by KCL at the node with potential V_M, we get the relation expression in Eq. 11.

$$C_{BM}V_B + C_{GMTx}V_T + C_{GMRx}V_R - (C_{MG} + C_{GMRx} + C_{GMTx} + C_{BM})V_M = 0 \quad (11)$$

Hence, the induced potential on the metallic object (V_M) is presented in Eq. 12.

$$V_M = \frac{C_{BM}}{C_A}V_B + \frac{C_{GMRx}}{C_A}V_R + \frac{C_{GMTx}}{C_A}V_T \quad (12)$$

where,

$$C_A = (C_{MG} + C_{GMRx} + C_{GMTx} + C_{BM}) \quad (12a)$$

For a large object, the expression for C_A can be approximately simplified as $C_A \approx (C_{MG} + C_{BM})$ (Since, C_{GMRx}, C_{GMTx} $<< C_{MG}$, C_{BM}). The coupling between the body-to-metallic object (C_{BM}) changes with the change in the average distance and orientation of subject relative to the metallic object. Now,

by KCL at the node with potential V_R, we get the relation expression in Eq. 13.

$$C_{L(eff.)}V_B-(C_{L(eff.)}+C_{xRx}+C_{GMRx})V_R-C_{GMRx}V_M=0 \tag{13}$$

Since, the subject's body potential (V_B) also changes under the influence of metallic objects in the surroundings. Incorporating the effect from the surrounding metals, the nodal voltage at the ground of the Rx is expressed in Eq. 14.

$$V_R=\frac{B}{P}V_B+\frac{Q}{P}V_T \tag{14}$$

where P, Q, and B take the following form:

$$P=\frac{1}{C_{L(eff.)}}\left[(C_{L(eff.)}+C_{xRx}+C_{GMRx})-\frac{C_{GMRx}^2}{C_A}\right] \tag{14a}$$

$$Q=\frac{C_{GMRx}C_{GMTx}}{C_{L(eff.)}C_A} \tag{14b}$$

$$B=1+\frac{C_{GMRx}C_{BM}}{C_{L(eff.)}C_A} \tag{14c}$$

$$C_{L(eff.)}=C_{GBRx}+C_L \tag{14d}$$

A generalized circuit model for the interaction between

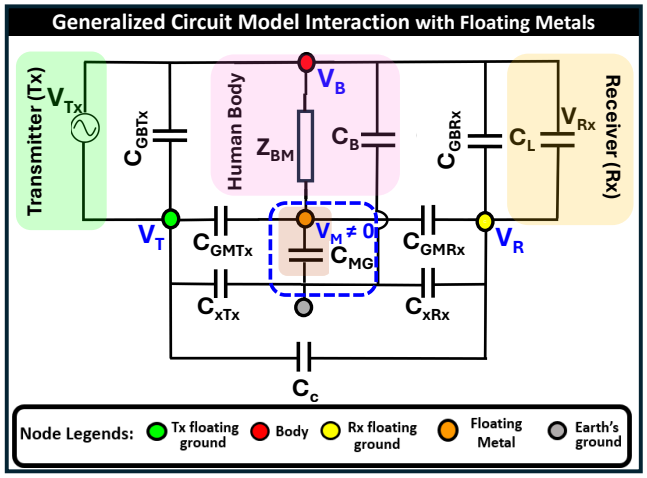

Fig. 4: Generalized circuit model for interaction between subject and Floating metallic obejcts.

EQS HBC user and a floating metallic object is presented in Supplementary Fig. 4. By KCL at node M, we obtain the expression for V_B in relation to V_M, V_T, and V_R, presented in Eq. 15.

$$V_B=\left(1+s\left(C_{GMRx}+C_{GMTx}+C_{MG}\right)Z_{BM}\right)V_M - s\,C_{GMRx}\,Z_{BM}\,V_R-s\,C_{GMTx}\,Z_{BM}\,V_T \tag{15}$$

By KCL at the ground node of the Rx, we obtain another equation relating V_R with V_B and V_M, presented in Eq. 16.

$$V_R\left(C_{xRx}+C_{L(\text{eff.})}+C_{GMRx}\right)=C_{L(\text{eff.})}\,V_B+C_{GMRx}\,V_M \tag{16}$$

Again, by KCL at the ground node, we obtain another expression relating V_B, V_R and V_T, presented in Eq. 17.

$$C_BV_B+C_{xRx}V_R+C_{xTx}V_T=0 \tag{17}$$

where, V_T can be expressed as

$$V_T=-(\frac{C_B}{C_{xTx}}V_B+\frac{C_{xRx}}{C_{xTx}}V_R) \tag{17a}$$

By substituting V_T from Eq. 17a in the expression for V_B in Eq. 15, we obtain

$$V_B=\frac{D}{A}V_M+\frac{F}{A}V_R \tag{18}$$

where A, D and F are defined in Eq. 18 (a, b, c)

$$A=1-sC_{GMTx}Z_{BM}\frac{C_B}{C_{xTx}} \tag{18a}$$

$$D=1+s(C_{GMRx}+C_{GMTx}+C_{MG})Z_{BM} \tag{18b}$$

$$F=(sC_{GMTx}\frac{C_{xRx}}{C_{xTx}}-sC_{GMRx})Z_{BM} \tag{18c}$$

Now, V_{Tx} can be written in relation to V_B and V_T, expressed in Eq. 19.

$$V_{Tx}=V_B-V_T \tag{19}$$

Substituting V_T and rearranging terms, we get

$$V_{Tx}=UV_B+TV_R \tag{19a}$$

where U and T are defined in Eq. 19 (b, c)

$$U=1+\frac{C_B}{C_{xTx}} \tag{19b}$$

$$T=\frac{C_{xRx}}{C_{xTx}} \tag{19c}$$

Now, V_M can be expressed in terms of V_B and V_R, presented in Eq. 20 can be written as

$$V_M=SV_B+RV_R \tag{20}$$

where S and R are defined in Eq. 20 (a, b)

$$S=-\frac{C_{L(eff.)}}{C_{GMRx}} \tag{20a}$$

$$R=\frac{C_{xRx}+C_{L(eff.)}+C_{GMRx}}{C_{GMRx}} \tag{20b}$$

Hence, the transfer function is formulated in Eq. 21

$$T_{NTFM}(s)=\frac{V_{Rx}}{V_{Tx}}=\frac{V_B-V_R}{V_B-V_T}\approx\left(\frac{1-\frac{(A-DS)}{DR+F}}{U+T\frac{(A-DS)}{DR+F}}\right) \tag{21}$$

Similar to grounded metal, during touch-based interaction with floating metal, the transfer characteristics ($T_{TFM}(s)$) can be obtained by substituting the expression of Z_{BM} from Eq. 7.

IV. Derivation of the Sensitivity Analysis

Since, the channel transfer function is defined as

$$T=\frac{V_{\text{Rx}}}{V_{\text{Tx}}}=\frac{V_B}{V_{Tx}}\times\frac{V_{Rx}}{V_B} =\frac{C_{\text{retTx}}}{C_{\text{retTx}}+C_{\text{Body}}}\times\frac{C_{\text{retRx}}}{C_{\text{retRx}}+C_{\text{L(eff.)}}}$$

The relative sensitivity of T to a small change in C_i is expressed in Eq. 22

$$S_{C_i}=\frac{C_i}{T}\frac{\partial T}{\partial C_i} \tag{22}$$

A. Sensitivities of $\frac{V_B}{V_{Tx}}$

$$\frac{\partial\left(\frac{V_B}{V_{Tx}}\right)}{\partial C_{\mathrm{retTx}}} = \frac{C_{\mathrm{Body}}}{\left(C_{\mathrm{retTx}} + C_{\mathrm{Body}}\right)^2} \tag{23a}$$

$$\frac{\partial\left(\frac{V_B}{V_{Tx}}\right)}{\partial C_{\mathrm{Body}}} = -\frac{C_{\mathrm{retTx}}}{\left(C_{\mathrm{retTx}} + C_{\mathrm{Body}}\right)^2} \tag{23b}$$

Hence, the relative sensitivities are defined in Eq. 23c, 23d.

$$S_{C_{\mathrm{retTx}}} = \frac{C_{\mathrm{retTx}}}{\left(\frac{V_B}{V_{Tx}}\right)} \frac{\partial\left(\frac{V_B}{V_{Tx}}\right)}{\partial C_{\mathrm{retTx}}} = \frac{C_{\mathrm{Body}}}{C_{\mathrm{retTx}} + C_{\mathrm{Body}}} \tag{23c}$$

$$S_{C_{\mathrm{Body}}} = \frac{C_{\mathrm{Body}}}{\left(\frac{V_B}{V_{Tx}}\right)} \frac{\partial\left(\frac{V_B}{V_{Tx}}\right)}{\partial C_{\mathrm{Body}}} = -\frac{C_{\mathrm{Body}}}{C_{\mathrm{retTx}} + C_{\mathrm{Body}}} \tag{23d}$$

B. Sensitivities of $\frac{V_{Rx}}{V_B}$

$$\frac{\partial\left(\frac{V_{Rx}}{V_B}\right)}{\partial C_{\mathrm{retRx}}} = \frac{C_{\mathrm{L(eff.)}}}{\left(C_{\mathrm{retRx}} + C_{\mathrm{L(eff.)}}\right)^2} \tag{24a}$$

$$\frac{\partial\left(\frac{V_{Rx}}{V_B}\right)}{\partial C_{\mathrm{L(eff.)}}} = -\frac{C_{\mathrm{retRx}}}{\left(C_{\mathrm{retRx}} + C_{\mathrm{L(eff.)}}\right)^2} \tag{24b}$$

$$S_{C_{\mathrm{retRx}}} = \frac{C_{\mathrm{retRx}}}{\left(\frac{V_{Rx}}{V_B}\right)} \frac{\partial\left(\frac{V_{Rx}}{V_B}\right)}{\partial C_{\mathrm{retRx}}} = \frac{C_{\mathrm{L(eff.)}}}{C_{\mathrm{retRx}} + C_{\mathrm{L(eff.)}}} \tag{24c}$$

$$S_{C_{\mathrm{L(eff.)}}} = \frac{C_{\mathrm{L(eff.)}}}{\left(\frac{V_{Rx}}{V_B}\right)} \frac{\partial\left(\frac{V_{Rx}}{V_B}\right)}{\partial C_{\mathrm{L(eff.)}}} = -\frac{C_{\mathrm{L(eff.)}}}{C_{\mathrm{retRx}} + C_{\mathrm{L(eff.)}}} \tag{24d}$$

The combined sensitivity can be obtained by putting these sensitivities expressed in Eqs. 23c, 23d, 24c, 24d, together and is expressed in Eqs. 25 and 25a.

$$\frac{\partial T}{\partial C_i} = \left(\frac{V_{Rx}}{V_B}\right) \frac{\partial\left(\frac{V_B}{V_{Tx}}\right)}{\partial C_i}, \quad C_i \in \{C_{\mathrm{retTx}}, C_{\mathrm{Body}}\} \tag{25}$$

$$\frac{\partial T}{\partial C_j} = \left(\frac{V_B}{V_{Tx}}\right) \frac{\partial\left(\frac{V_{Rx}}{V_B}\right)}{\partial C_j}, \quad C_j \in \{C_{\mathrm{retRx}}, C_{\mathrm{L(eff.)}}\} \tag{25a}$$

V. Electric Field Variation inside Elevator

The variations in the coupled E-Field strength from the subject's body to the walls of the metallic enclosure for different positions of the subject inside an elevator are illustrated in Supplementary Fig. 5. Considerable reduction in the coupled E-field strength on the subject's body is observed when the human leans on the elevator face wall through the torso.

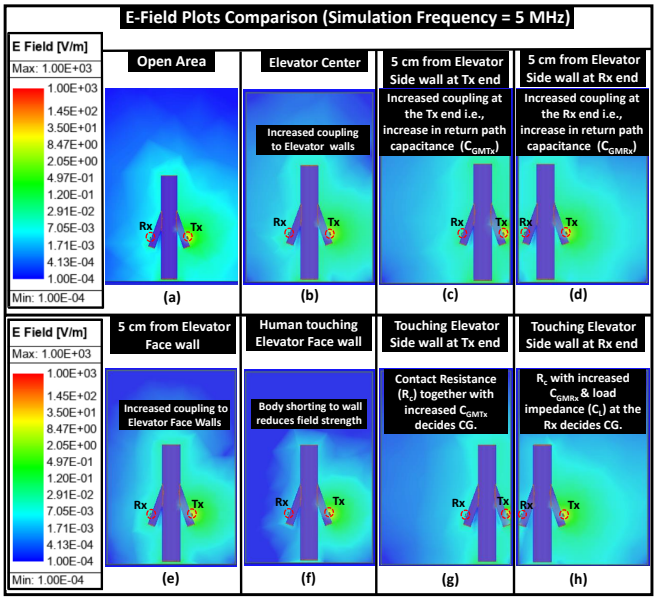

Fig. 5: Comparative analysis of the E-Field plots under different scenarios in metallic enclosure: The following scenarios are illustrated: (a) In an Open Area, (b) At the elevator center, (c) 5 cm from the wall at the Tx end, (d) 5 cm from the wall at the Rx end, (e) Subject's torso is at 5 cm from face wall, (f) Subject is leaning on the face wall, (g) Human touching side wall at the Tx side, (h) human touching side wall at the Rx side.

VI. Performance Analysis of the Communication Channel

The presence of metallic objects within the leakage limit (∼5 cm from the subject's body and ∼20 cm from communication devices, such as the transmitter (Tx) and receiver (Rx)) affects the parasitic return paths of Electro-quasistatic (EQS) Human Body Communication (HBC). This phenomenon is expected to impact the performance of wireless body-centric communication. In this analysis, we investigate the impact of nearby metallic objects on the performance of the body channel by examining variations in Signal-to-Noise Ratio (SNR), Shannon capacity, and bit error rate for different modulation schemes. These schemes include On-Off Keying (OOK), commonly referred to as Pulse Amplitude Modulation (PAM-2), Quadrature Amplitude Modulation (QAM), and Binary Phase Shift Keying (BPSK). We assume a white noise floor of 5 nV/$\sqrt{\mathrm{Hz}}$. Let the nominal return-path capacitances and body capacitances be $\mathrm{C_{xTx}}$, $\mathrm{C_{xRx}}$, and $\mathrm{C_B}$, and let the metal-induced perturbations be $\mathrm{C_{GMTx}}$, $\mathrm{C_{GMRx}}$, and $\mathrm{C_{Body}}$. Then the net capacitances become $\mathrm{C_{retTx}}$, $\mathrm{C_{retRx}}$, and $\mathrm{C_{Body}}$ The resulting EQS-HBC channel gain is presented in Eq. 26.

$$T = \frac{C_{\mathrm{retTx}}}{C_{\mathrm{retTx}} + C_{\mathrm{Body}}} \times \frac{C_{\mathrm{retRx}}}{C_{\mathrm{retRx}} + C_{\mathrm{L(eff.)}}} \tag{26}$$

Assume a transmit RMS voltage $\mathrm{V_{Tx}}$ and white noise power spectral density (PSD): $\mathrm{N_0} = \left(5 \times 10^{-9}\right)^2 = 25 \times 10^{-18}\mathrm{V^2/Hz}$. Over an operational channel bandwidth B, the noise variance is $\mathrm{N_0B}$. The received signal power (P_{sig}) is

presented in Eq. 27

$$P_{\text{sig}} = \left|TV_{\text{Tx}}\right|^2 \quad P_{\text{noise}} = N_0\, B \tag{27}$$

From the Eq. 26 and 27 the obtained SNR is presented in Eq. 28.

$$SNR = \frac{P_{\text{sig}}}{P_{\text{noise}}} = \frac{|T|^2\, V_{\text{Tx}}^2}{N_0\, B} \tag{28}$$

Hence, from the obtained SNR and bandwidth, the channel capacity is expressed in Eq. 29

$$\text{Channel Capacity (bits/s)} = B \log_2(1 + SNR) \tag{29}$$

Now, the BER expressions for various modulation schemes as a function of SNR are presented in Eqs. 30a, 30b, 30c.

$$\text{BER}_{\text{OOK}} = Q\left(\sqrt{\gamma}\right) \tag{30a}$$

$$\text{BER}_{\text{QPSK}} = Q\left(\sqrt{2\,\gamma}\right) \tag{30b}$$

$$\text{BER}_{M\text{-QAM}} = \frac{4(\sqrt{M}-1)}{\sqrt{M}\,\log_2 M}\, Q\left(\sqrt{\frac{3\,\gamma\,\log_2 M}{M-1}}\right) \tag{30c}$$

where Q is defined in Eq. 30d

$$Q(x) = \frac{1}{\sqrt{2\pi}} \int_x^{\infty} e^{-t^2/2}\, dt \tag{30d}$$

in the above expressions γ is related to SNR by how bit-energy over the noise band. In particular, transmitting at bit-rate of R_b over a noise bandwidth B, the signal power is defined as $\text{P}_\text{s}\text{ig} = \text{E}_\text{b}\,\text{R}_\text{b}$, hence the SNR is expressed in Eq. 31.

$$\frac{P_{sig}}{P_{noise}} = \frac{E_b\, R_b}{N_0\, B} = \frac{E_b}{N_0} \cdot \frac{R_b}{B} \tag{31a}$$

$$\gamma = \frac{E_b}{N_0} = SNR \times \frac{B}{R_b} \tag{31b}$$

Assuming the bit-rate to be the same as operational bandwidth ($R_b = B$), we get $\gamma = SNR$.

Now, with operational bandwidth (B) of 5 MHz, $\text{V}_{\text{Tx}} =$ 1V, assuming a noise floor of -70 dBV for CMOS-based body-communication receiver, capacitances (C_{xTx}, C_B, C_{xRx}, $\text{C}_{\text{L(eff.)}}$) being (0.2, 150, 0.2, 5) pF in open area, if the surrounding metal induced perturbations being Δ (C_{xTx}, C_B, C_{xRx}, $\text{C}_{\text{L(eff.)}}$): (0.8, 0, 0.8, 0) pF, i.e., (C_{retTx}, C_{Body}, C_{retRx}, $\text{C}_{\text{L(eff.)}}$): (1, 150, 1, 5) pF, $T \approx 0.0013$, $SNR \approx 12.49$ dB. Over a bandwidth of 5 MHz, channel capacity comes around 21.1 Mbps. The the ideal-coherent BER for OOK comes 1 $\times\ 10^{-5}$ that satisfies the intended uncoded BER requirements for OOK (10^{-2}). The variation in performance metrics with the change in C_{retTx} and C_{Body} is captured in Supplementary Fig. 6. In summary, it can be interpreted as, an increase in C_{retTx} leads to an enhanced channel capacity (i.e., $\sim$10 Mbps increase in channel capacity with 100% increase in C_{retTx}) from the improved SNR, illustrated in Supplementary Fig. 6(a). The variation in ideal-coherent BER with C_{Body} for different modulation schemes like OOK, QPSK, and 16-QAM, presented in Supplementary Fig. 6(b), shows an increase in C_{Body} facilitates reliable communication at reduced BER. On contrary, a rise in C_{Body} reduces the channel capacity owing to an attenuation in SNR, represented in Supplementary Fig. 6(c). The BER also exhibit an increasing trend with increasing C_{Body}, shown in Supplementary Fig. 6 (d).

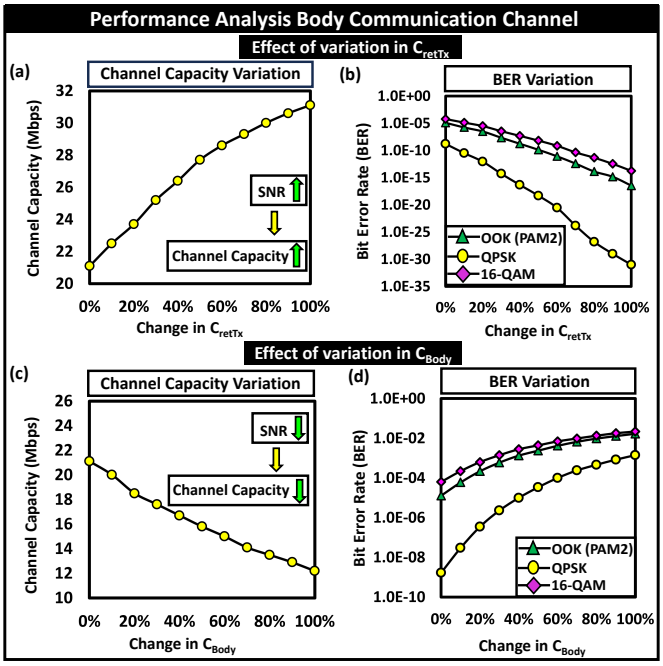

Fig. 6: Analyzing the effect of variation in C_{retTx} and C_{Body} on the performance metrics like channel capacity, Bit-error rate (BER) for EQS HBC: (a) Channel capacity variation with C_{retTx}, (b) BER variation with C_{retTx}, (c) Channel capacity variation with C_{Body}, (d) BER variation with C_{Body}

This research focuses on the scientific and system validation of the effect of nearby metals on electrostatic human body communication (EQS HBC), and data collection from humans of different generalize across body types (e.g., BMI, height, skin properties) was not needed and/or performed. A study on the variability of the communication channel for EQS HBC across different users was previously conducted. It was inferred that in EQS, with the operating wavelength (λ) being several orders of magnitude higher than the maximum body channel length (i.e., $l_{Body} << \lambda$), the electrically distributed characteristics of the body can be fairly approximated as a lumped conductor specifically as an electrical lossy wire and these subject-specific variabilities remain within the tolerance limit of the designed transceiver system. Thus, even if the channel loss varies slightly, EQS-HBC lumped model adapts seamlessly across diverse users. Calibration via a small set of measurements refines tissue resistivity and fringe-field factors, yielding a predictive, personalized HBC channel model. The variabilities can be tackled by designing adaptive transceiver system, even if the transmission loss changes with the subject body dimension..

The transmission characteristics are likely to vary with the dynamic activities of EQS HBC users, such as walking and arm swinging. These activities can alter parasitic capacitive coupling with surrounding metallic objects especially change in subject's body posture i.e., limb angles (θ) or torso posture (h) may alter the return path capacitances of the devices ($C_{xTx}(\theta), C_{xRx}(\theta)$), and subsequently the capacitance between the devices and user's body i.e., $C_{GBRx}(\theta)$ and body-to-earth capacitance $C_B(h, \theta)$. A study by Yang et al. [7] ex-

amined the variability of communication channel performance for EQS HBC with subject's posture, particularly through arm movement, which can affect the extent of inter-device coupling and body shadowing, depending on the relative separation between the transmitter and receiver and their proximity to the user's torso. Our study did not account for these factors in our simulations or experiments, as the primary focus of this fundamental study was to investigate the impact of nearby metals ranging from non-grounded, grounded metallic objects to enclosed metallic surroundings like elevators and cars on transmission loss of EQS HBC. We recognize that the challenges posed by dynamic movements could be addressed by designing a posture-aware adaptive transceiver system, which can effectively handle these variabilities with an appropriate link margin. This insight motivates future work in this area.

Differentiating Touch and near touch

The quantitative threshold that differentiates between two interactions can be understood in terms of the impedance Z_{BM} between a subject's body and a metallic object. This impedance can be modeled as a resistance R_{BM} in parallel with a capacitance C_{BM}, presented in Eq. 32.

$$Z_{BM} = \frac{R_{BM}}{1 + j\,\omega\,C_{BM}} \tag{32}$$

For simplicity, if we assume the capacitance between the subject's body and a nearby metal, $C_{BM}(d)$, as a function of distance d—and approximate it as a parallel-plate capacitor (neglecting fringe effects) with overlapping area A—we obtain Eq. 33.

$$C_{BM}(d) \approx \frac{\varepsilon_0\,\varepsilon_r\,A}{d} \tag{33}$$

Here $\varepsilon_0 = 8.85 \times 10^{-12}\,\mathrm{F/m}$ is the permittivity of free space, and ε_r is the relative permittivity. Define d_c as the critical distance that separates "near touch" ($d_c > 0$) from "touch" ($d_c = 0$) interactions. During a "near touch" ($d_c > 0$), the capacitive branch dominates ($1/(j\omega C_{BM}) \ll R_{BM}$) and the impedance reduces to Eq. 32.

$$Z_{BM} = \frac{1}{j\,\omega\,C_{BM}} \approx \frac{d}{j\,\omega\,\varepsilon_0\,\varepsilon_r\,A} \tag{34}$$

Consequently, within the electro-quasistatic regime the channel transfer function for capacitive Human Body Communication remains nearly flat. In contrast, during a "touch" interaction ($d_c = 0$), the coupling impedance falls below the contact resistance R_{con}. We set $R_{BM} = R_{\mathrm{con}}$, which depends on the contact area A_{con}:

$$R_{\mathrm{con}} \propto \frac{1}{A_{\mathrm{con}}} \tag{35}$$

At the boundary $d = d_c$, $|Z_{BM}(d)| \approx R_{\mathrm{con}}$, giving

$$d_c \approx \omega\,\varepsilon_0\,\varepsilon_r\,A\,R_{\mathrm{con}} \tag{36}$$

Thus if the subject approaches closer than d_c, the capacitive impedance matches a true touch and the system can no longer distinguish "near-touch" from contact. As an example, at f = 5 MHz, with $A = 10\ \mathrm{cm}^2$, $R_{\mathrm{con}} = 1\ \mathrm{k\Omega}$. Eq. 36 yields

$$d_c \approx 0.278\ \mathrm{mm}$$

showing that the critical distance lies in the sub-millimeter to millimeter range. When the subject actually contacts a ground-connected metallic object, the presence of R_{con} introduces a frequency-dependent high-pass behavior. The cutoff frequency f_c varies as

$$f_c \propto \frac{1}{\sqrt{R_{\mathrm{con}}}}.$$

If instead the metal is floating, one still sees high-pass characteristics; with sufficiently good contact (larger A_{con}, smaller R_{con}), the voltage drop across R_{con} becomes negligible and the transfer function again flattens.

Additional Details of Experimental Setup

A. Calibration of Wearable Transmitter

With its ground being floating, the wearable Tx requires to be calibrated against a benchtop ground-connected standard. By connecting the transmitter to a benchtop oscilloscope while varying its frequency in the EQS regime from 100 kHz to 20 MHz, the peak-peak voltage shown in the oscilloscope is recorded, and the calibration correction for the Tx is calculated.

B. Calibration of Wearable Receiver:

The receiver is calibrated by connecting it to a Keysight signal generator, a benchtop standard. The output power of the benchtop signal generator varied over different power levels while varying the frequency from 100 kHz to 20 MHz, and the power difference observed between the two devices is noted to calculate the correction factor for the tinySA.

C. Calibration of Buffer:

The buffer's input connects to the output of a benchtop function generator, while the buffer's output is connected to a benchtop signal analyzer. The buffer's correction factor is then recorded.

The buffer circuit is made by using OPA2836 from Texas Instruments which is an ultra-low power, rail-to-rail output swing, voltage-feedback operational amplifier. It operates with a supply voltage ranging in 2.5 V to 5.5 V, with its unity gain bandwidth (UGB) of 205 MHz, slew rate of 560 V/μs and its input voltage noise sensitivity of 4.6 nV/$\sqrt{Hz}$ making it suitable for handling ac signals with desired sensitivity at the receiver. For applications with battery-powered wearable devices where power is a key importance, the low-power consumption and high-frequency performance of the OPA2836 offers superior performance. We agree that a buffer circuit can attenuate the signal, however, with its higher UGB, this op-amp based buffer circuit designed at a unity gain configuration can handle 5 MHz input. We want to emphasize that this study uses operating frequency of 5 MHz to remain within the EQS frequency range. All the numerical simulations and experiments were conducted at this frequency.

D. Signal coupler at Tx & Rx

The signal coupler at Tx and Rx side is made of a commercially available double-sided conductive copper foil tape, measuring 3.5 cm × 4.5 cm, and of < 0.1 cm thickness, affixed to the bottom surface of the cut-board, ensures contact with the subject's skin.

E. System Schematic Diagram

The schematic of the measurement system shown in Fig. 7 illustrates the signal processing pipeline.

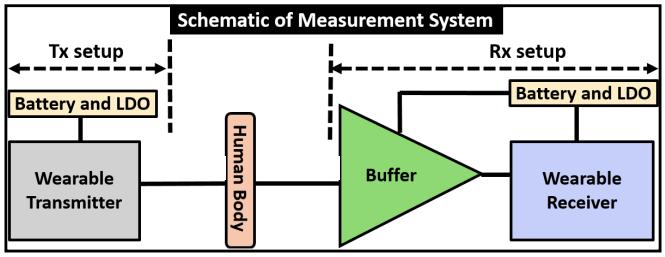

Fig. 7: The wearable transmitter (Tx) with its signal coupler in contact with the user's skin couples EQS signal to the body. A capacitive receiver (Rx) at the wrist of another arm is used to measure received voltage. The receiver setup includes the Tiny SA spectrum analyzer together with Buffer, c. Customized Buffer with high impedance capacitive termination for voltage mode communication

F. Test Conditions

Since the focus of this study is evaluating the communication channel's performance in various metallic surroundings, experiments for grounded and non-grounded metallic objects are conducted in standard laboratory environments at an average temperature of 27°C (80.6 °F) and humidity 65% and the experiments in metallic enclosures are conducted in elevators and cars. We agree that performing measurements inside an anechoic chamber offers a controlled, low noise setting for acquiring precise frequency response data. Nonetheless, the chamber is surrounded by a grounded metal enclosure, which influences the results in the low-frequency EQS region. This grounded enclosure enhances the overall return path capacitance, leading to a decrease in channel loss. Consequently, the EQS region displays reduced loss, and the crossover points between the EQS and EM regions shift to higher frequencies. The anechoic chamber is capable of effectively absorbing incident electromagnetic (EM) waves above 80 MHz; thus, the findings obtained in the chamber can only be reliably compared with HFSS open-air simulations at frequencies higher than 80 MHz, as suggested by Nath et al.

Moreover, skin impedance (Z_{skin}) is affected by humidity and sweat, which can raise the received voltage (V_{Rx}). However, variations in Z_{skin} impact V_{Rx} by less than 3 dB at EQS frequencies due to high impedance return paths of capacitive EQS HBC with wearable devices. Temperature shifts tissue permittivity and conductivity, but these effects are minor at EQS frequencies and hence these variabilities can be tackled by designing transceivers with suited link margin. Therefore, ambient Electro-magnetic Interference, humidity, and temperature do not significantly affect SNR, bandwidth, or channel capacity of EQS HBC.

Signal dispersion in body channel communication can occur due to two main factors: (a) amplitude distortion, which involves frequency-dependent attenuation, and (b) phase distortion (or group-delay distortion), which refers to frequency-dependent delays. The dominance of either factor at low versus high at EQS frequencies depends on the specific channel model being used. Considering the RC-Line model of the Body channel i.e., the body path (transmitter (Tx)-skin-tissue-skin-receiver(Rx)) as a distributed RC line, it can be shown that the amplitude attenuation grows as $\propto \sqrt{\omega}$; phase shift also grows as $\propto \sqrt{\omega}$ where $\omega = 2\pi f$, f = operating frequency. In capacitive electro quasistatic human body communication (EQS HBC), the human body serves as the forward path for signal transmission, while the parasitic coupling capacitance between the device's ground and the earth's ground functions as the return path. This configuration creates a closed loop for the body channel as an electrical circuit. It is worth mentioning Maity et al. demonstrated that the transmission loss through the body in the forward path is approximately 6-10 dB, depending on whether single-ended or differential excitation and termination are used. Hence the overall transmission loss is primarily influenced by the high impedance return paths in a scenario where both the transmitter (Tx) and receiver (Rx) are wearable devices. Furthermore, it was found that using high-impedance capacitive termination at the receiver leads to flat band channel characteristics in the EQS frequency domain. Hence, this flat band channel characteristic can be leveraged to reduce the effect of signal distortion from the channel. In contrast, the galvanic mode of HBC experiences higher degree of signal distortion from the tissue properties as the principle of operation lies in dipole-dipole coupling i.e., the electric field lines of the Tx dipole get weakened by the surrounding tissues before getting picked up at the Rx dipole and the extent of this enhances at higher operating frequencies. Moreover, the nonlinearities introduced from the electrode-skin interface remain considerably lower at EQS frequencies as it was shown that the voltage drop across the band-to-skin impedance ($Z_{band-skin} < 100\Omega$ where $Z_{band-skin} = R_{band}||C_{band}$ where $R_{band} = 100\Omega, C_{band} = 200pF$) can be ignored in comparison to the voltage across the high impedance return paths ($Z_{C_xTx}, Z_{C_xRx} > 100k\Omega$).

VII. Schematic Illustration of the Experimental Scenarios

This section provides a schematic representation of the experimental scenarios involving the interaction between an EQS HBC subject and the elevator walls, as illustrated in Supplementary Fig. 8. The proximity to the elevator walls affects the parasitic return path capacitances, resulting in variations in transmission loss. The scenarios depicted in Supplementary

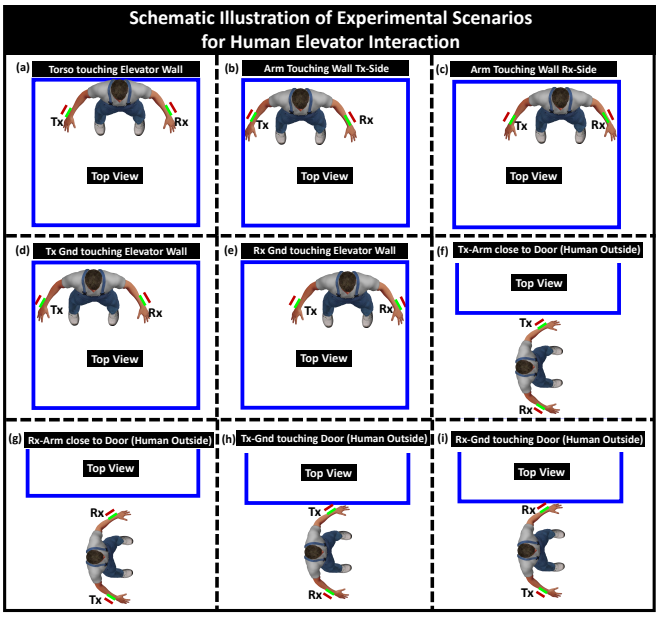

Fig. 8: Experimental Scenarios of interaction between EQS HBC user & Elevator: (a) Torso touching elevator wall, (b) Arm touching wall Tx-Side, (c) Arm touching wall Rx-Side, (d) Ground of Tx touching elevator wall, (e) Ground of Rx touching elevator wall, (f) Arm with Tx close to Door (Human Outside), (g) Arm with Rx close to Door (Human Outside), (h) Ground of Tx touching Door (Human Outside), (i) Ground of Rx touching Door (Human Outside)

Figs. 8 (a, b, c) shows changes in the locations of touch-based interactions between the subject and the elevator walls. In contrast, Supplementary Figs. 8 (d, e) presents scenarios where the ground of the transmit (Tx) and receive (Rx) components comes into contact with the elevator walls. Supplementary Figs. 8 (f, g) illustrates proximity-based interactions when the individual is outside. Finally, Supplementary Figs. 8 (h, i) depicts scenarios where the ground of the Tx and Rx components makes contact with the elevator door while the person is outside. This section presents a diagrammatic representation of the experimental setup involving the interaction between an EQS HBC subject and a vehicle, as illustrated in Supplementary Fig. 9. The subject's distance from the car door affects the parasitic return path capacitances, resulting in changes in transmission loss. The scenario depicted in Supplementary Fig. 9 (a) illustrates the subject seated in the middle seat of the car. In contrast, Supplementary Figs. 9 (b, c) showcase situations where the ground connections of the transmit (Tx) and receive (Rx) components make contact with the car door. Supplementary Figs. 9 (d, e) demonstrates the situation when the subject reaches their arm out of the car window. Lastly, Supplementary Fig. 9 (f) portrays scenarios in which the subject stands outside the vehicle.

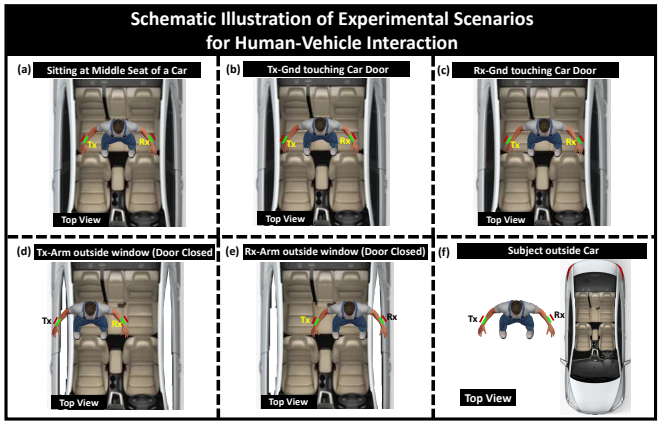

Fig. 9: Experimental Scenarios of interaction between EQS HBC user & Car: (a) Subject seating at middle seat of the car, (b) Ground of the Tx touching car door, (c) Ground of Rx touching car door, (d) Arm with Tx outside car window (Door Closed), (e) Arm with Rx outside car window (Door Closed), (f) Subject outside car